Ephexin1 Is Required for Structural Maturation and Neurotransmission at the Neuromuscular Junction

Lei Shi,[1,2,3] Busma Butt,[1,2,3] Fanny C.F. Ip,[1,2,3] Ying Dai,[1,2,3] Liwen Jiang,[4,5] Wing-Ho Yung,[6] Michael E. Greenberg,[7] Amy K.Y. Fu,[1,2,3] and Nancy Y. Ip[1,2,3,*]

[1]Department of Biochemistry
[2]Molecular Neuroscience Center
[3]State Key Laboratory of Molecular Neuroscience
The Hong Kong University of Science and Technology, Clear Water Bay, Hong Kong SAR, China
[4]Department of Biology
[5]Molecular Biotechnology Program
[6]School of Biomedical Sciences
The Chinese University of Hong Kong, Shatin, NT, Hong Kong SAR, China
[7]Department of Neurobiology, Harvard Medical School, 300 Longwood Avenue, Boston, MA 02115, USA
*Correspondence: boip@ust.hk
DOI 10.1016/j.neuron.2010.01.012

SUMMARY

The maturation of neuromuscular junctions (NMJs) requires the topological transformation of postsynaptic acetylcholine receptor (AChR)-containing structures from a simple plaque to an elaborate structure composed of pretzel-like branches. This maturation process results in the precise apposition of the presynaptic and postsynaptic specializations. However, little is known about the molecular mechanisms underlying the plaque-to-pretzel transition of AChR clusters. In this study, we identify an essential role for the RhoGEF ephexin1 in the maturation of AChR clusters. Adult *ephexin1*$^{-/-}$ mice exhibit severe muscle weakness and impaired synaptic transmission at the NMJ. Intriguingly, when ephexin1 expression is deficient in vivo, the NMJ fails to mature into the pretzel-like shape, and such abnormalities can be rescued by re-expression of ephexin1. We further demonstrate that ephexin1 regulates the stability of AChR clusters in a RhoA-dependent manner. Taken together, our findings reveal an indispensible role for ephexin1 in regulating the structural maturation and neurotransmission of NMJs.

INTRODUCTION

Efficient neurotransmission depends on the precise alignment of neurotransmitter release sites at presynaptic nerve terminals with neurotransmitter receptors in the postsynaptic compartment. At the adult vertebrate neuromuscular junction (NMJ), the acetylcholine receptor (AChR)-enriched postsynaptic muscle membrane is organized into a topologically elaborate structure that is perfectly aligned with the branching of the motor neuron terminal (Sanes and Lichtman, 2001). Both the presynaptic and postsynaptic sites undergo remarkable changes during early postnatal development before the NMJ achieves its mature, complex shape (Sanes and Lichtman, 2001). Postsynaptically, the initial, small oval-like AChR clusters with uniform receptor density are transformed into multiperforated, elaborate branches that have a pretzel-like shape (Balice-Gordon and Lichtman, 1993; Kummer et al., 2004; Lanuza et al., 2002; Marques et al., 2000; Slater, 1982). The topological maturation of the postsynaptic apparatus occurs when the muscle membrane invaginates to form primary and secondary folds. These maturational changes at the postsynaptic muscle membrane are believed to be required for efficient neuromuscular transmission and normal motor function. It has been well documented that impaired formation of synaptic folds is a hallmark of a number of neuromuscular disorders including myasthenia gravis (Selcen et al., 2008; Slater, 2008; Slater et al., 2006). Furthermore, perturbation of the maturation of AChR clusters into the pretzel-like structure has been observed in mouse models of congenital myasthenic syndromes or neuromuscular diseases such as spinal muscular atrophy (Chevessier et al., 2008; Kong et al., 2009). These findings highlight a pivotal role of the postsynaptic maturation in the maintenance of normal neuromuscular responses. However, the detailed molecular mechanisms underlying the transformation of the NMJ into a topologically complex pretzel-like structure are still poorly understood.

Although *trans*-synaptic activity has been suggested to play a role in the remodeling of the postsynaptic region of the NMJ (Balice-Gordon and Lichtman, 1994), the topological transformation of AChR clusters was recently found to occur in a nerve-independent manner (Kummer et al., 2004). Laminins, the major components of the basal lamina at the synaptic clefts of NMJs, have been demonstrated to act directly on muscle cells to promote postsynaptic maturation (Nishimune et al., 2008). This laminin-induced event is mediated by the increased aggregation of components of the dystrophin-glycoprotein complex (DGC), a cytoskeletal protein complex that is critical for the stabilization of AChR clusters and the structural maintenance of the NMJ (Adams et al., 2004; Grady et al., 2000). Indeed, proteins such as the DGC that control the stability of AChR clusters are believed to be crucial in the process of NMJ maturation, because selective receptor regions are programmed to be disassembled

to generate the multiperforated pretzel-like shape of the mature NMJ (Balice-Gordon and Lichtman, 1993; Kummer et al., 2004; Lanuza et al., 2002; Marques et al., 2000; Slater, 1982).

It has been well established that the anchorage of AChRs to the postsynaptic actin cytoskeletal network is critical for regulating the stability of AChR clusters (Mitsui et al., 2000). Several cytoplasmic proteins, including rapsyn, src-family kinases (SFKs), and the heat shock protein 90β, stabilize AChR clusters by enhancing the linkage between AChRs and the cytoskeleton (Luo et al., 2008; Moransard et al., 2003; Sadisivam et al., 2005). Furthermore, polymerization of the actin cytoskeleton is important for the formation and stabilization of the AChR clusters (Dai et al., 2000; Hoch et al., 1994). Importantly, the clustering/ disassembly of AChR clusters is suggested to depend on actin depolymerizing factor (ADF)/cofilin-directed receptor trafficking to the postsynaptic membrane (Lee et al., 2009). Moreover, key regulators of actin dynamics, including members of the small Rho GTPase family and their effector Pak1, regulate agrin-induced clustering of AChRs in cultured myotubes (Luo et al., 2003; Luo et al., 2002; Weston et al., 2000, 2003). A heat shock protein homolog Tid1 has recently been reported to mediate agrin-induced activation of Rho GTPases and to regulate AChR clustering (Linnoila et al., 2008). Nonetheless, the precise roles of Rho GTPases in regulating the stability of AChR clusters, and the key mechanisms that modulate their activities during NMJ maturation, remain unclear. A Rho guanine nucleotide exchange factor (GEF), ephexin1, has previously been demonstrated to be a downstream effector of EphA4 signaling, linking EphA4 to actin cytoskeletal dynamics through enhancement of RhoA activation (Fu et al., 2007; Sahin et al., 2005; Shamah et al., 2001). Indeed, ephexin1 activation is important for EphA4-dependent axon guidance and synaptic maintenance (Fu et al., 2007; Sahin et al., 2005; Shamah et al., 2001). Given the expression of EphA4 at the adult NMJ and the implication that EphA4-dependent signaling might regulate postsynaptic development of the NMJ (Lai et al., 2004; Lai et al., 2001), we were interested to investigate the function of ephexin1 at the NMJ.

In this study, we have identified ephexin1 as a key regulator of postsynaptic maturation of NMJs. Adult ephexin1$^{-/-}$ mice displayed muscle weakness and impaired neuromuscular transmission associated with NMJ abnormalities including a simplified morphology of AChR clusters and an imprecise synaptic apposition of the presynaptic and postsynaptic portions of the NMJ. Detailed morphological analysis of the NMJs in ephexin1$^{-/-}$ mice revealed that the AChR clusters failed to transform into the pretzel-like structure that is a hallmark of mature NMJs. Taken together, our findings reveal an essential role of ephexin1 in the postsynaptic maturation of NMJs.

RESULTS

Adult ephexin1$^{-/-}$ Mice Display Severe Muscle Weakness and Impaired Neuromuscular Transmission

To examine whether ephexin1 plays a key role in regulating the function of the NMJ, we performed a number of behavioral analyses to assess whether there are neuromuscular deficits in ephexin1$^{-/-}$ mice. We found that ephexin1$^{-/-}$ mice have a comparable body size, body weight, and survival rate to that

of wild-type littermates during postnatal life (data not shown). However, the adult mutant mice showed impairment in the Rota-Rod test, which evaluates the motor coordination and muscle fatigue of the animals. These mutant mice displayed a significantly shorter latency of falling off from the accelerating Rota-Rod (Figure 1A). To study whether this behavioral deficit is caused by muscle weakness, we assessed the limb muscle strength of the mutant mice via the inverted screen test, in which the animals are required to support their body weight by grasping a wire grid. Intriguingly, the duration for which the mutant mice remained on the screen was significantly shorter when compared to that of the wild-type littermates (Figure 1B), indicative of severe muscle weakness in the ephexin1$^{-/-}$ mice. Furthermore, consistent with the reduced muscle strength, ephexin1$^{-/-}$ mice displayed reduced locomotor activity in the open field test, shown by the significantly reduced distance traveled by the mutant mice as compared to that of their wild-type littermates (Figure S1 available online). To examine whether the muscle weakness of ephexin1$^{-/-}$ mice is a consequence of impaired neuromuscular function, we compared synaptic transmission at the NMJs of wild-type and ephexin1$^{-/-}$ mice using electrophysiology. Interestingly, the amplitude of spontaneous miniature endplate potentials (MEPPs) in adult ephexin1$^{-/-}$ mice was significantly decreased when compared to that of wild-type mice (Figures 1C–1F). Furthermore, the rise time of mutant MEPPs showed a much broader range, and was significantly prolonged when compared to that of the wild-type (Figures 1D and 1F). These results strongly suggest that the neurotransmission at ephexin1$^{-/-}$ NMJs is impaired, leading to muscle weakness in the ephexin1$^{-/-}$ mice.

NMJs of Adult ephexin1$^{-/-}$ Mice Exhibit Morphological and Ultrastructural Abnormalities

The decreased amplitude as well as the altered rise time kinetics of the MEPPs of the ephexin1$^{-/-}$ mice suggested that the postsynaptic development of NMJs in these mice might be abnormal. Thus, we examined the morphology of NMJs in the ephexin1$^{-/-}$ mice by staining for presynaptic and postsynaptic components. Intriguingly, whereas AChR clusters at wild-type NMJs displayed a mature pretzel-like pattern characterized by an elaborate array of branches, AChR clusters at the ephexin1$^{-/-}$ NMJs exhibited a much more simplified structure with shortened and discontinuous branches (Figure 2A). Quantitative analysis showed that a higher proportion of NMJs in ephexin1$^{-/-}$ mice appeared as discrete patches of AChR clusters (~70% contained ≥7 discrete AChR regions) when compared to that of wild-type (~40%; Figure 2B). More importantly, the synaptic alignment at the ephexin1$^{-/-}$ NMJ was disrupted: AChR clusters in the ephexin1$^{-/-}$ mice failed to align precisely with nerve terminals, and axon terminals were frequently found to extend beyond the borders of AChR clusters (Figure 2A). Quantitative analysis showed that both the percentage of AChRs colocalized with nerve terminals and the percentage of nerve terminals colocalized with AChRs were significantly reduced at adult ephexin1$^{-/-}$ NMJs (Figures 2C and 2D). We next examined whether there are ultrastructural alterations at ephexin1$^{-/-}$ NMJs via electron microscopy analysis. Interestingly, abnormalities in the morphology of the postsynaptic membrane were observed
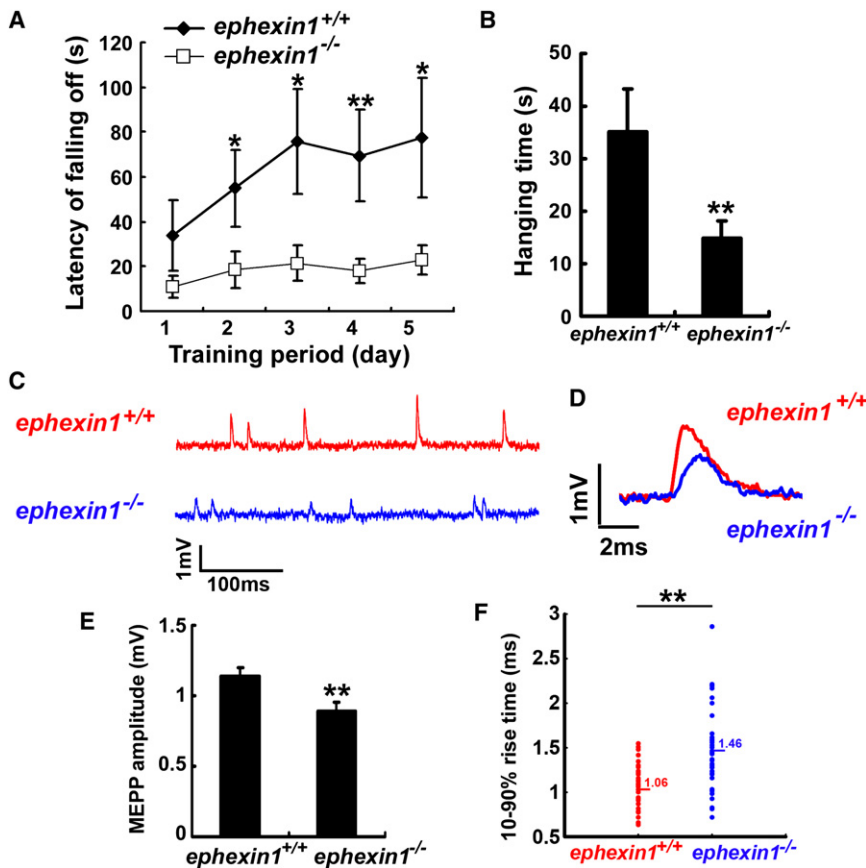
Figure 1. *ephexin1*$^{-/-}$ Mice Display Muscle Weakness and Impaired Neuromuscular Transmission

(A) *ephexin1*$^{-/-}$ mice showed compromised ability in the Rota-Rod test during 5 days of training. The total time over which the mice remained on the rotating rod before falling off was measured. n = 20 for *ephexin1*$^{+/+}$ and n = 12 for *ephexin1*$^{-/-}$ mice. Mean ± SEM, *p < 0.05, **p < 0.01, Student's t test.

(B) *ephexin1*$^{-/-}$ mice showed forelimb muscle weakness. The duration of time the mice can hang on to the inverted wire mesh before falling off was measured. n = 24 for *ephexin1*$^{+/+}$ and n = 28 for *ephexin1*$^{-/-}$ mice. Mean ± SEM, **p < 0.01, Student's t test.

(C–F) *ephexin1*$^{-/-}$ mice exhibited impaired neuromuscular transmission. Hemidiaphragms of adult wild-type and *ephexin1*$^{-/-}$ mice were prepared for recording the spontaneous miniature endplate potentials (MEPPs). (n = 36 from eight wild-type mice; n = 39 from seven *ephexin1*$^{-/-}$ mice.) Typical responses of the MEPPs were presented in both long time frame (100 ms; C) and short time frame (2 ms; D). (E) Pooled data showing that the amplitude of *ephexin1*$^{-/-}$ MEPPs is significantly reduced. Mean ± SEM, **p < 0.01, Student's t test. (F) Data are presented as a scatter plot showing prolonged and more variable rise time kinetics of *ephexin1*$^{-/-}$ MEPPs. **p < 0.01, Student's t test.

See also Figure S1.

in *ephexin1*$^{-/-}$ NMJs (Figures 2E–2G). The wild-type muscle membrane is characterized by numerous evenly distributed junctional folds with comparable depth, and each of these folds is generally oriented directly toward the synaptic cleft (Figures 2E and 2F). In contrast, junctional folds at the *ephexin1*$^{-/-}$ NMJs are poorly organized, showing varied depth, curved or shortened fragments, and disorientation relative to the synaptic cleft (Figures 2E and 2F). Moreover, the mutant folds displayed a more variable distance from one another, and quantification revealed that the average density of the synaptic folds was significantly decreased in *ephexin1*$^{-/-}$ mice (Figure 2G).

Postnatal Maturation of AChRs Is Impaired in *ephexin1*$^{-/-}$ Mice

To investigate whether the neuromuscular defects observed in *ephexin1*$^{-/-}$ mice are due to perturbed formation or maturation processes of the NMJ, we began to examine the expression pattern of ephexin1 during muscle development. We found that ephexin1 protein is prominently expressed in mouse muscle at late embryonic stages, and is downregulated during postnatal development (Figure S2A). Similarly, ephexin1 protein expression is downregulated in cultured C2C12 cells upon myotube formation (Figure S2B). We next examined the spatial distribution of ephexin1 at the NMJ during postnatal development. Whereas ephexin1 protein colocalized with AChR clusters at the junctional regions of muscle at postnatal day 7 (P7), ephexin1 was also detected at the extrajunctional regions surrounding

AChRs (Figure S2C). As the NMJ matures, the extrasynaptic localization of ephexin1 was found to be significantly reduced and the protein became enriched within the synaptic sites (at P14 and adult, Figure S2C). Interestingly, immunostaining analysis of whole-mount P2 diaphragm preparations revealed that both presynaptic and postsynaptic differentiation, including nerve sprouting, the endplate band width, and the number and size of AChR clusters, were grossly normal in *ephexin1*$^{-/-}$ mice (Figure S3A and Table S1 available online), suggesting that ephexin1 is not essential for the initial formation of NMJs.

We then asked whether ephexin1 affects the postnatal maturation of NMJs. Postsynaptic AChR clusters are normally plaque-shaped at birth, and then undergo a transformation to a perforated, and eventually a mature pretzel-like, morphology during the postnatal period (Kummer et al., 2004; Lanuza et al., 2002; Marques et al., 2000; Slater, 1982). To investigate whether ephexin1 regulates this process, we compared the morphology of AChR clusters in whole-mount preparations from both wild-type and *ephexin1*$^{-/-}$ tibialis anterior muscle during the first 3 postnatal weeks. Both the size and morphology of AChR clusters observed in newborn *ephexin1*$^{-/-}$ mice were similar to those observed in wild-type mice (Figure S3A and Table S1). However, AChR clusters in *ephexin1*$^{-/-}$ mice displayed progressive morphological abnormalities during postnatal development (Figure 3A). The area of AChR clusters in *ephexin1*$^{-/-}$ mice was notably larger (∼15%) than those of wild-type mice during the first 2 postnatal weeks (P5–P14) (Figure 3B and Table S1).
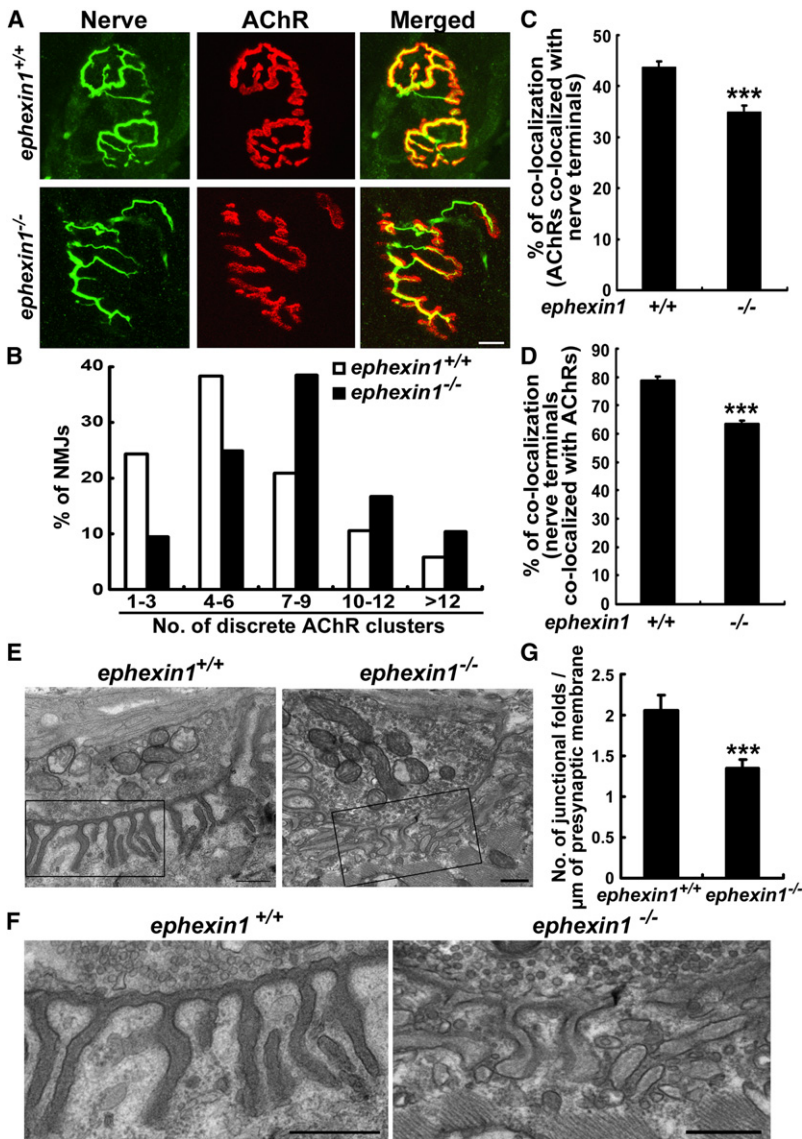
Figure 2. Adult *ephexin1*⁻/⁻ Mice Exhibit Abnormal NMJ Structure

(A–D) Individually teased sternomastoid muscle fibers of adult *ephexin1*⁻/⁻ mice and those of their corresponding wild-type littermates were costained with anti-synaptophysin and neurofilament antibodies for presynaptic axon terminals (Nerve; green) and α-BTX for postsynaptic AChR clusters (red). (A) AChR clusters in *ephexin1*⁻/⁻ mice appeared to be more discontinuous. (B) The number of discrete AChR regions per NMJ was counted, and data are presented as percentages of NMJs that contain indicated numbers of discrete AChR regions (n = 86 from five *ephexin1*⁺/⁺ mice; n = 96 from five *ephexin1*⁻/⁻ mice). Scale bar, 10 μm. (C and D) *ephexin1*⁻/⁻ NMJs showed imprecise synaptic apposition. Data are presented as the colocalization of AChRs with nerve terminals (percentage of red pixels that are also green; C), or nerve terminals with AChRs (percentage of green pixels that are also red; D). Mean ± SEM is given; ***p < 0.005, Student's t test (n = 36 from five *ephexin1*⁺/⁺ mice; n = 53 from five *ephexin1*⁻/⁻ mice).

(E–G) *ephexin1*⁻/⁻ NMJs exhibit ultrastructural abnormalities. Tibialis anterior muscle from adult wild-type and *ephexin1*⁻/⁻ mice was prepared for electron microscopic analysis. Representative images are shown in lower magnification (E), and the corresponding boxed regions are shown in higher magnification for visualization of the junctional folds (F). The *ephexin1*⁻/⁻ junctional folds display abnormal morphology such as shortened, curved, fragmented, or disorientated phenotype. Scale bars, 500 nm. (G) The density of postsynaptic folds was decreased in *ephexin1*⁻/⁻ NMJs. Mean ± SEM, ***p < 0.005, Student's t test.

See also Figure S2.

Interestingly, the area of AChR clusters at wild-type NMJs decreased after reaching a peak at P14 (Figure 3B and Table S1), likely due to a rapid loss of AChR receptor regions within the postsynaptic apparatus during topological maturation. However, this reduction in the area of AChR clusters after P14 was not observed in *ephexin1*⁻/⁻ mice (Figure 3B and Table S1). Similar results were obtained when the sternomastoid muscles of wild-type and *ephexin1*⁻/⁻ mice were compared (data not shown). The enlargement of AChR clusters during early postnatal stages in *ephexin1*⁻/⁻ mice suggests that the normal disassembly of AChR regions is impaired in these mice.

Selective loss of receptors within the AChR plaque results in the formation of receptor-free regions, leading to the perforated appearance of mature AChR clusters. This process is believed to be crucial for the topological maturation of AChR clusters (Balice-Gordon and Lichtman, 1993; Marques et al., 2000). To further demonstrate that the enlargement of AChR cluster area in postnatal *ephexin1*⁻/⁻ mice is a consequence of impaired disassembly of AChR clusters, we examined the perforation of AChRs during NMJ maturation. Interestingly, the percentage of perforated AChR clusters was notably reduced in *ephexin1*⁻/⁻ mice during the second and third postnatal weeks (P10–P11 to P17–P18; Figure 3C), suggesting that the absence of ephexin1 leads to a defect in the loss of AChRs within postsynaptic regions during postnatal maturation. Consistent with the increased number of plaque-like AChR clusters in *ephexin1*⁻/⁻ mice, a higher percentage of the NMJ area was occupied by AChRs in these mutant mice at P17–P18 (Figure 3D), indicative of reduced disassembly of AChR clusters within individual NMJs. More strikingly, while most of the AChR clusters (~70%) in P17–P18 wild-type mice exhibited the characteristic pretzel-like shape with elaborate arrays of branches, only a small portion of AChR clusters in *ephexin1*⁻/⁻ mice (~15%) acquired this pretzel-like shape (Figure 3E). In contrast, most of the *ephexin1*⁻/⁻ AChR clusters remained in various immature forms, including those unable to form branches with either sharp borders or ring-like morphology (~70%), or even those with an undifferentiated plaque-like appearance (~15%; Figure 3E). These findings suggest that the maturation of AChR clusters to form complex, branched arrays is severely perturbed in *ephexin1*⁻/⁻ mice.
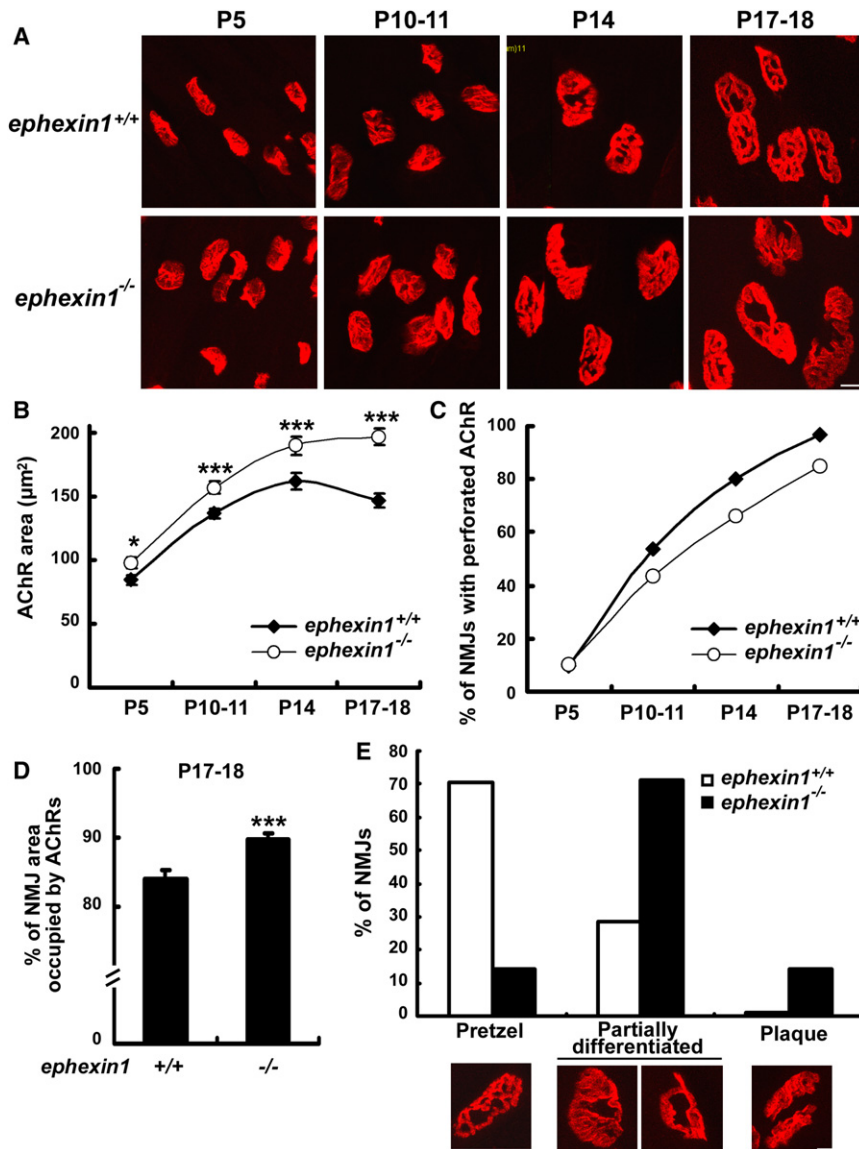
Figure 3. Postnatal Maturation of AChR Clusters Is Perturbed in *ephexin1*⁻/⁻ Mice

(A) Whole-mount preparations of tibialis anterior muscle from wild-type and *ephexin1*⁻/⁻ mice at postnatal stages as indicated were stained for postsynaptic AChR clusters with α-BTX.

(B) The area of AChR clusters was enlarged in *ephexin1*⁻/⁻ mice upon postnatal development. Mean ± SEM, *p < 0.05, ***p < 0.005, Student's t test. Detailed quantification analysis was shown in Table S1.

(C and D) NMJs in *ephexin1*⁻/⁻ mice were less complex than those of wild-type mice. (C) Fewer NMJs in *ephexin1*⁻/⁻ mice were perforated (n ≥ 78 from three *ephexin1*⁻/⁻ or wild-type mice at each stage). (D) Postsynaptic area occupied by AChR clusters increased significantly in *ephexin1*⁻/⁻ mice at P17–P18 (n = 71 from three *ephexin1*⁺/⁺ mice; n = 97 from three *ephexin1*⁻/⁻ mice). Data are presented as the percentages of NMJ area occupied by AChR clusters (area of AChR/NMJ area). Mean ± SEM is given; ***p < 0.005, Student's t test.
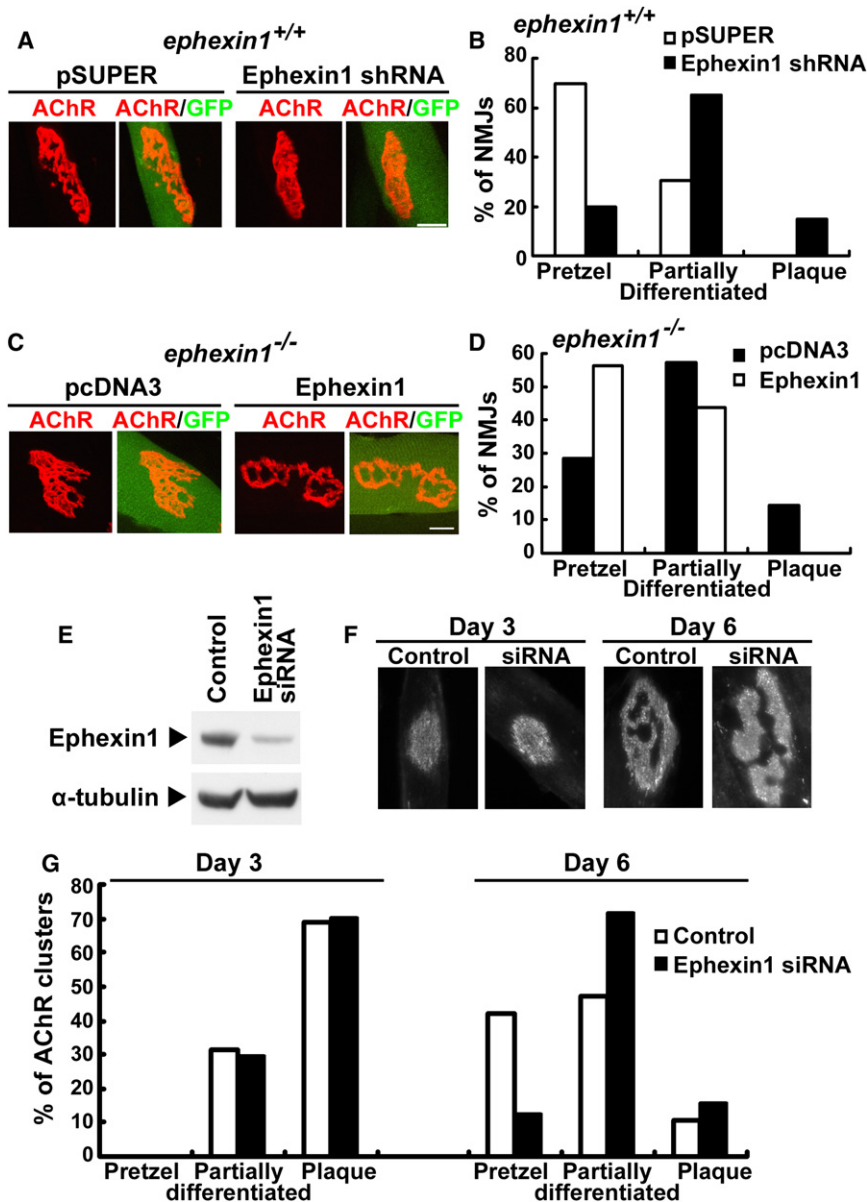
(E) AChR clusters failed to develop into mature pretzel-like shapes in *ephexin1*⁻/⁻ mice. Photomicrographs depicted the characteristic morphology of AChRs at P17–P18. AChR clusters were grouped into three subtypes according to their appearance: pretzel, partially differentiated (only a portion of the AChR clusters are pretzel-like or ring-like), and plaque. Data are presented as the percentages of NMJs in each subtype (n = 102 from three *ephexin1*⁺/⁺ mice; n = 118 from three *ephexin1*⁻/⁻ mice). Scale bars, 10 μm.

See also Figure S3 and Table S1.

Ephexin1 Functions Postsynaptically to Regulate AChR Maturation

Although presynaptic activity has long been suggested to influence the postsynaptic development of the NMJ, formation of the topologically complex postsynaptic apparatus can occur in vitro even in the absence of innervation through a series of transitions similar to the maturational events observed in vivo (Kummer et al., 2004). To examine whether muscle ephexin1 is required for AChR maturation, we either functionally knocked down ephexin1 expression with RNAi or re-expressed wild-type ephexin1 in mutant muscles and examined the effect on AChR clustering. We first silenced ephexin1 expression in the tibialis anterior muscle of P6–P7 mice by injection of pSUPER ephexin1 shRNA, which was previously demonstrated to functionally knock down endogenous ephexin1 expression (Fu et al., 2001). The ephexin1-silenced muscle fibers were identified by the coexpression of green fluorescent protein (GFP)

(Figure 4A). Consistent with our observations in *ephexin1*⁻/⁻ mice, knockdown of ephexin1 resulted in an increased percentage of immature AChR clusters that were either partially differentiated (∼65%) or remained in a plaque-like shape (∼15%) at P18 (Figures 4A and 4B). This observation, together with the findings that there was an enlargement of the AChR area and a higher percentage of NMJs occupied by AChRs in ephexin1-knockdown muscle (Figures S4A and S4B), suggests that ephexin1 deficiency specifically in muscle results in aberrant maturation of the NMJ. Intriguingly, re-expression of ephexin1 in the *ephexin1*⁻/⁻ tibialis anterior muscle is sufficient to restore the normal AChR maturation, resulting in an increased number of pretzel-shaped AChR clusters (∼60%) and resemblance to the phenotype observed in wild-type mice (Figures 4C and 4D). In addition, the size of the AChR clusters and the percentage of NMJs occupied by AChRs in the ephexin1-injected mutant muscle were similar to those observed in wild-type mice (Figures S4C and S4D).

To further elucidate the role of muscle ephexin1, we examined the maturation of AChR clusters in aneurally cultured myotubes (Kummer et al., 2004). Consistent with our in vivo observations

Figure 4. Postsynaptic Maturation of the NMJ Is Regulated by Muscle-Expressed Ephexin1

Tibialis anterior muscle fibers of P7 *ephexin1*^{+/+} or *ephexin1*^{−/−} mice were injected with pSUPER ephexin1 shRNA, or ephexin1 expression construct, correspondingly, together with GFP construct. Whole-mount preparations of these muscles were examined at P18 by α-BTX staining for AChR clusters.

(A and B) Knockdown of ephexin1 in mouse muscle results in impaired maturation of AChR clusters. (A) Representative images. (B) Quantification analysis of NMJs displaying pretzel-like, partially differentiated, or plaque-like shape. (n = 23 from seven mice injected with pSUPER; n = 20 from eight mice injected with ephexin1 shRNA.)

(C and D) Re-expression of ephexin1 in *ephexin1*^{−/−} muscle restores the maturation of AChR clusters. (C) Representative images. (D) Percentage of NMJs displaying pretzel-like, partially differentiated, or plaque-like shape (n = 11 from five *ephexin1*^{−/−} mice injected with pcDNA3; n = 17 from five mice injected with ephexin1). Scale bars: 10 μm.

(E–G) Maturation of AChR clusters in aneurally cultured myotubes was inhibited by suppression of ephexin1 expression. (E) Western blot analysis showing successful knockdown of ephexin1 in C2C12 myotubes by ephexin1 siRNA. α-tubulin acts as a control for equal protein loading. (F and G) Whereas formation of plaque-like AChR clusters was not affected by ephexin1 knockdown, maturation of these clusters into pretzel-like shapes was largely inhibited. (F) Representative images. (G) Quantification analysis of AChR clusters displaying pretzel-like, partially differentiated, or plaque-like shapes. (~100–200 AChR clusters from three separate experiments are examined in control or ephexin1-knockdown myotubes.)

See also Figure S4.

that *ephexin1*^{−/−} mice failed to develop mature pretzel-shaped AChR clusters, the silencing of ephexin1 expression in myotubes by siRNA (Figure 4E) did not perturb the formation of plaques in the early development of myotubes (Day 3), but substantially inhibited the subsequent maturation process, resulting in failed transformation of AChR clusters into a pretzel-like shape (Day 6) (Figures 4F and 4G). This result suggests that ephexin1-mediated AChR maturation does not require synaptic activity. Together, these findings demonstrate that muscle ephexin1 is required for the topological maturation of AChR clusters at NMJs.

Ephexin1 Destabilizes AChR Clusters through Regulating the Cytoskeletal Linkage of the Receptors

The increased area of AChR clusters observed in *ephexin1*^{−/−} NMJs suggests that ephexin1 plays a regulatory role in the dispersal of AChR regions. To investigate the underlying mechanisms, we first examined whether ephexin1 regulates the stability of AChR clusters in cultured C2C12 myotubes. Previous studies have shown that whereas treatment of C2C12 myotubes with agrin induces robust clustering of AChRs, removal of agrin leads to dispersal of AChR clusters. Interestingly, we found that knockdown of ephexin1 in myotubes did not affect agrin-induced AChR clustering, but did attenuate the dispersal of preexisting AChR clusters (Figures 5A and 5B). The number of AChR clusters that remained in ephexin1-knockdown myotubes following agrin removal was significantly higher than that observed in the control myotubes (Figures 5A and 5B). These findings demonstrate that ephexin1 is important for the dispersal of preexisting AChR clusters in myotubes, which is consistent with the in vivo role of ephexin1 in postnatal disassembly of AChR clusters. Because AChR clusters are suggested to be stabilized through linkage to the postsynaptic cytoskeleton network, we examined whether ephexin1 promotes dispersal of AChR
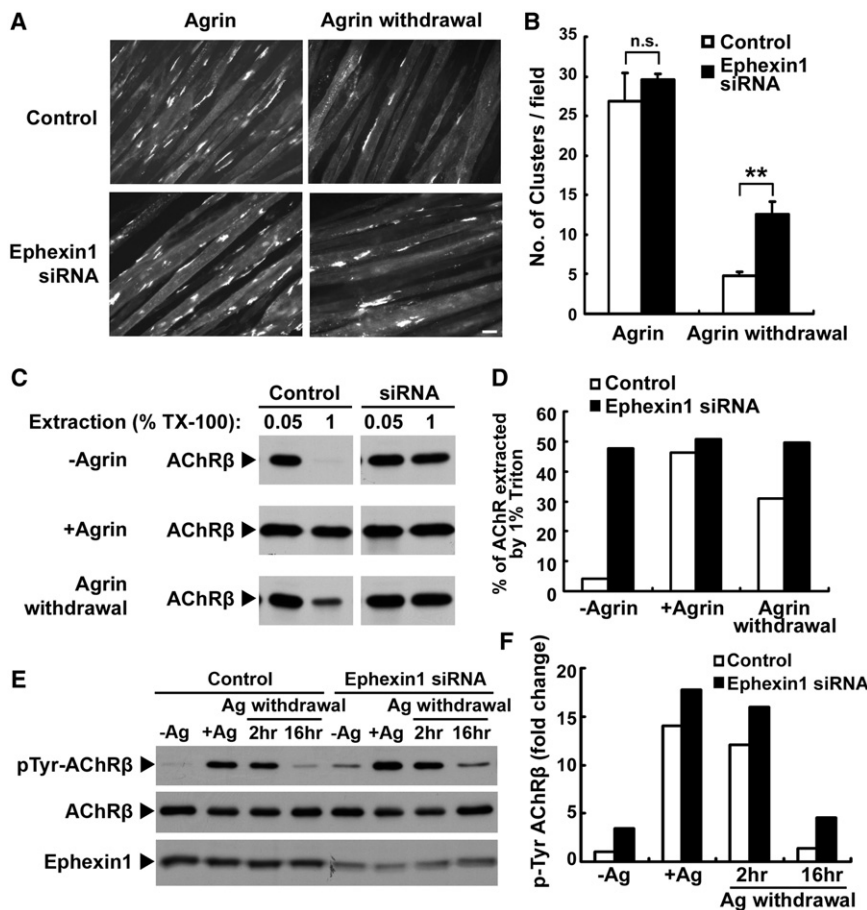
Figure 5. Knockdown of Ephexin1 Inhibits the Dispersal of Preexisting AChR Clusters in C2C12 Myotubes through Organization of the Cytoskeletal Anchorage of the Receptors

(A and B) Knockdown of ephexin1 did not affect agrin-induced AChR clustering, but did inhibit the dispersal of preexisting AChR clusters. C2C12 myotubes transfected with ephexin1 siRNA were treated with agrin for 16 hr (Agrin), and then stained with α-BTX for AChR clusters. Alternatively, ephexin1-knockdown myotubes were treated with agrin for 8 hr to induce clustering of AChRs, which were then labeled by α-BTX. Subsequently, myotubes were washed and then maintained in agrin-free medium for an additional 12–14 hr (Agrin withdrawal). Representative images (A) and quantification (B) of AChR clusters on myotubes from each condition are shown. Scale bar, 20 μm. Mean ± SEM of at least three experiments is given. (n.s. = not significant, p > 0.05, ephexin1 siRNA versus control siRNA upon agrin treatment; **p < 0.01, ephexin1 siRNA versus control siRNA upon agrin withdrawal, Student's t test).

(C and D) The linkage of the AChR clusters to cytoskeleton was enhanced in ephexin1-knockdown myotubes. Myotubes were subjected to sequential extraction using different concentrations of Triton X-100 (first extracted with 0.05%, followed by 1% detergent). AChRs in the two fractions were precipitated by biotin-conjugated α-BTX, and subjected to western blot analysis for AChRβ subunit. (D) Percentage of AChRβ subunits extracted by the second extraction (1% Triton X-100).

(E and F) Enhanced tyrosine phosphorylation of AChRβ subunit in ephexin1-knockdown myotubes. Ephexin1-knockdown myotubes were incubated with agrin (+Ag), or followed by the withdrawal of agrin (Ag withdrawal). AChRs were precipitated and then subjected to western blot analysis using phosphotyrosine antibody (pTyr-AChRβ). AChRβ and ephexin1 were used as loading controls. (F) Fold change of pTyr-AChRβ.

clusters by attenuating the cytoskeletal anchorage of the receptors. We first assessed the relative strength of the interaction between AChRs and the cytoskeleton by a sequential detergent extraction (Sadasivam et al., 2005). Interestingly, we found that in both untreated myotubes and myotubes that were first treated with agrin followed by agrin removal, most of the AChRs in the control group were solubilized in the first extraction with milder detergent (Figures 5C and 5D). In contrast, around half of the population of AChRs in ephexin1-silenced myotubes were resistant to the first extraction, and could only be extracted with more stringent detergent conditions (Figures 5C and 5D). Furthermore, we found that tyrosine phosphorylation of AChRβ subunit, a signaling event associated with the cytoskeletal anchorage of the receptors (Borges and Ferns, 2001), was generally upregulated in untreated, agrin-treated, or agrin removal myotubes when ephexin1 expression is knocked down (Figures 5E and 5F). This enhanced receptor tyrosine phosphorylation, together with the decreased extractability of AChRs, suggests that in the absence of ephexin1 expression there is an increase in the strength of the link of AChR to the cytoskeleton, which then could lead to a decrease in the dispersal of AChR clusters in

ephexin1-deficient myotubes. Together, these data suggest that ephexin1 destabilizes AChR clusters by reducing the linkage of the AChR to the cytoskeleton.

Activation of Ephexin1 toward RhoA by Ephrin-A1 Promotes the Dispersal of AChR Clusters

We next examined whether activation of ephexin1 enhances the dispersal of AChR clusters. It has been reported that activation of EphA4 by its cognate ligand, ephrin-A1, enhances the GEF activity of ephexin1 toward RhoA (Fu et al., 2007; Sahin et al., 2005). We found that ephexin1 could be recruited to activated Eph receptors upon ephrin-A1 stimulation in C2C12 myotubes (Figure 6A). Moreover, ephrin-A1 treatment increases RhoA activity in an ephexin1-dependent manner (Figures 6B and 6C). Importantly, while ephrin-A1 treatment led to a significant reduction (∼30%) in the number of preexisting AChR clusters, knockdown of ephexin1 completely abolished this ephrin-A1-stimulated AChR dispersal (Figures 6D and 6E). This finding suggests that activation of ephexin1 by ephrin-A1 promotes the dispersal of AChR clusters. Consistent with previous observations (Figures 5A and 5B), knockdown of ephexin1 in
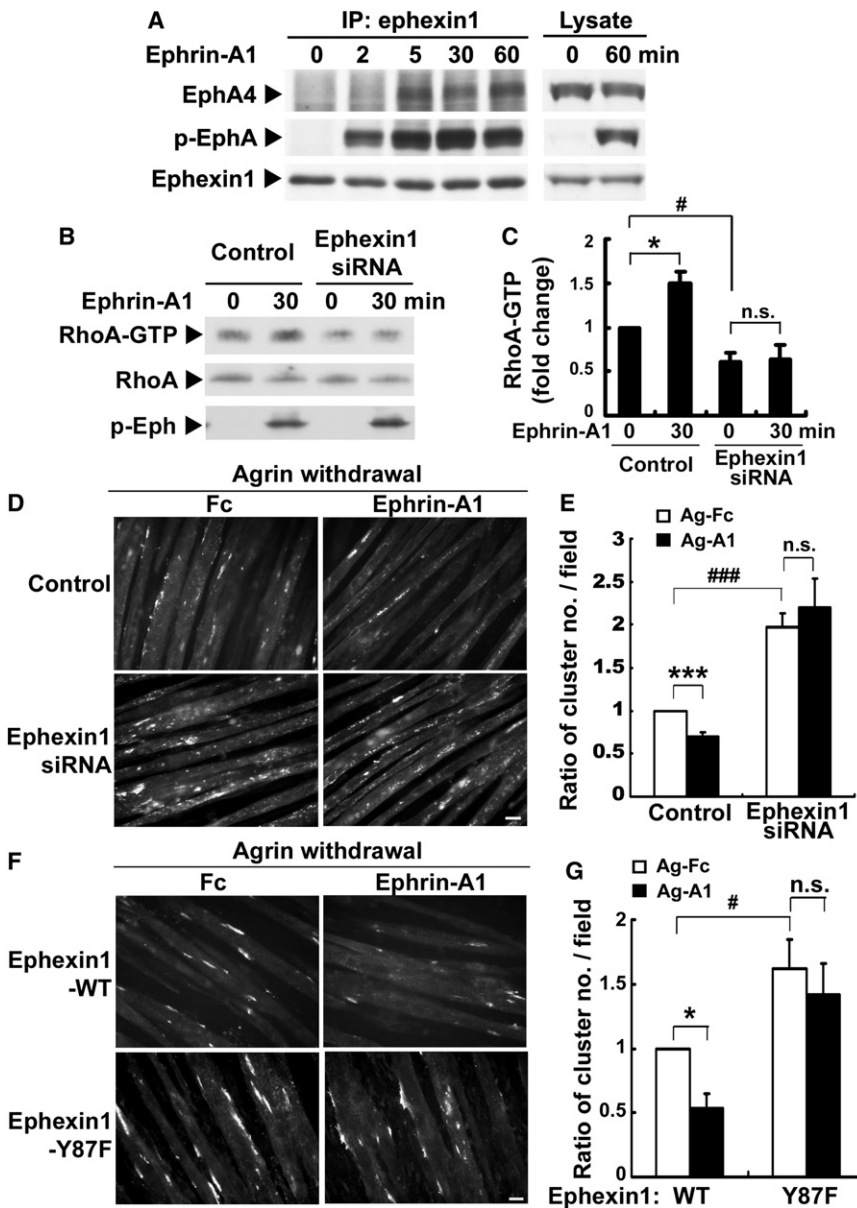
Figure 6. Activation of GEF Activity of Ephexin1 toward RhoA by Ephrin-A1 Enhances the Dispersal of AChR Clusters

(A) Ephexin1 was recruited to the activated EphA4 in cultured myotubes upon ephrin-A1 treatment. C2C12 myotubes were treated with ephrin-A1 for 0–60 min as indicated.

(B) Ephrin-A1 induced RhoA activation in myotubes in an ephexin1-dependent manner. Ephexin1-knockdown myotubes were treated with ephrin-A1 for 30 min, and the cell lysates were collected and subjected to RhoA activation assay.

(C) Quantification of the level of active RhoA (fold change). Mean ± SEM of at least three experiments is given. (*$p < 0.05$, ephrin-A1 treatment for 30 min versus 0 min in control myotubes; #$p < 0.05$, ephexin1 siRNA knockdown versus control at 0 min; n.s. = not significant, $p > 0.05$, ephrin-A1 treatment for 30 min versus 0 min in ephexin1-knockdown myotubes; Student's t test).

(D and E) Ephrin-A1 treatment enhanced the dispersal of AChRs in an ephexin1-dependent manner. Myotubes transfected with ephexin1 siRNA were first treated with agrin to induce AChR clustering. Following agrin withdrawal, myotubes were treated with ephrin-A1 or Fc for an additional 12–14 hr. Scale bar, 20 μm. (E) Data are represented as a ratio of the number of AChR clusters/field. Mean ± SEM of at least three experiments is given. (***$p < 0.005$, ephrin-A1 versus Fc in control myotubes; ###$p < 0.005$, ephexin1 siRNA versus control siRNA in Ag-Fc condition; n.s., $p > 0.05$, ephrin-A1 versus Fc treatment in ephexin1-knockdown myotubes, Student's t test).

(F and G) Inhibition of the exchange activity of ephexin1 toward RhoA abolished ephrin-A1-induced AChR cluster dispersal. C2C12 myotubes were transfected with mRNA encoding wild-type ephexin1 (WT) or its mutant (Y87F). Myotubes were treated with agrin and subsequently with ephrin-A1 as described above. (G) Data were represented as a ratio of AChR cluster number/field. Mean ± SEM of at least three experiments is given. (*$p < 0.05$, ephrin-A1 versus Fc in ephexin1-WT expressing myotubes; #$p < 0.05$, myotubes expressing ephexin1 Y87F versus WT in Ag-Fc condition; n.s., $p > 0.05$, ephrin-A1 versus Fc treatment in ephexin1-Y87F-expressing myotubes, Student's t test). Scale bars, 20 μm.
See also Figure S5.

myotubes alone was sufficient to stabilize AChR clusters (Figures 6D and 6E).

Activation of the RhoA-stimulating activity of ephexin1 is induced by ephrin-A/EphA4-dependent phosphorylation of ephexin1 at Tyr[87] (Sahin et al., 2005). Overexpression of the phosphorylation mutant of ephexin1 at Tyr[87] (Y87F) totally abolished the ability of ephrin-A1 to disperse AChR clusters (Figures 6F and 6G). Because ephexin1 Y87F blocks EphA activation of RhoA, these findings suggest that ephexin1-dependent RhoA activation is required for ephrin-A1-mediated AChR dispersal. Notably, similar to the effect of ephexin1 knockdown, expres-

sion of ephexin1 Y87F mutant in myotubes is sufficient to stabilize AChR clusters (Figures 6F and 6G). This suggests that phosphorylation of ephexin1 at Tyr[87] may be responsible for basal RhoA activation and AChR dispersal in myotubes. Furthermore, we found that blockade of RhoA-dependent signaling by Y-27632, a pharmacological inhibitor of the RhoA effector Rho-kinase (ROCK), abolished ephrin-A1-stimulated dispersal of AChR clusters (Figures S5A and S5B). Taken together, these findings suggest that ephexin1 mediates EphA-dependent dispersal of AChRs by a RhoA-dependent mechanism.
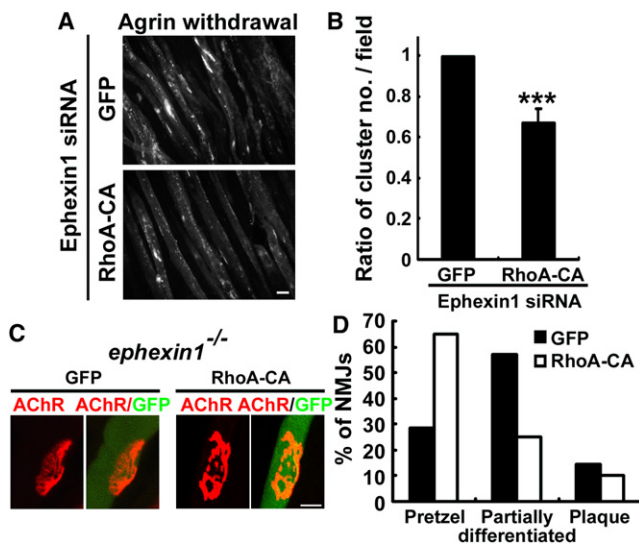
Figure 7. Ephexin1-Mediated Maturation of AChR Clusters Is Dependent on RhoA Activation

(A and B) Expression of a GFP-tagged constitutively active RhoA mutant (RhoA-CA) in ephexin1-knockdown myotubes enhanced the dispersal of AChR clusters. Myotubes expressing ephexin1 siRNA were treated with agrin to induce AChR clustering. Following agrin withdrawal, the ephexin1-knockdown myotubes were transfected with mRNA encoding RhoA-CA or GFP. Scale bar, 20 μm. (B) Data were presented as a ratio of AChR cluster number/field. Mean ± SEM of at least three experiments is given; ***p < 0.005, Student's t test.

(C and D) RhoA activation restores the maturation of AChR clusters in *ephexin1*$^{-/-}$ muscle. Tibialis anterior muscle fibers of P7 *ephexin1*$^{-/-}$ mice were injected with a GFP-tagged constitutively active RhoA mutant (RhoA-CA). Whole-mount preparations of these muscle fibers were stained for AChR clusters at P18 by α-BTX. (C) Representative images. Scale bar, 10 μm. (D) Percentage of NMJs displaying pretzel-like, partially differentiated, or plaque-like shape. (n = 11 from four *ephexin1*$^{-/-}$ mice injected with GFP, n = 20 from four *ephexin1*$^{-/-}$ mice injected with RhoA-CA)

Ephexin-Mediated Maturation of AChR Clusters Is Dependent on RhoA Activation

Strikingly, expression of constitutively active RhoA (RhoA-CA) in ephexin1-knockdown myotubes was sufficient to disperse preexisting AChR clusters, rescuing the knockdown effect of ephexin1 (Figures 7A and 7B). To address the role of RhoA in ephexin1-mediated AChR maturation, we injected the tibialis anterior muscle of P6–P7 *ephexin1*$^{-/-}$ mice with RhoA-CA. Intriguingly, more than 60% of the RhoA-CA-expressed muscle fibers displayed mature pretzel-shaped AChR clusters, indicating that RhoA-CA fully rescued the morphological defects of *ephexin1*$^{-/-}$ AChR clusters (Figures 7C and 7D). Thus, the ephexin1-mediated maturation of AChR clusters occurs via the activation of RhoA.

DISCUSSION

In this study, we provide evidence that the Rho GEF ephexin1 is essential for efficient synaptic maturation and transmission at the NMJ. We found that the transformation of AChR clusters from a simple oval shape to a mature pretzel-like morphology

is aberrant in *ephexin1*$^{-/-}$ mice during postnatal development. This impaired postsynaptic maturation likely accounts for the ultrastructural abnormalities and imprecise synaptic apposition observed in adult *ephexin1*$^{-/-}$ mice, and results in impaired neurotransmission and muscle weakness. Importantly, our findings reveal the essential role of ephexin1-mediated signaling in regulating the postsynaptic maturation through RhoA-dependent reorganization of the actin cytoskeleton at the postsynaptic membrane. Thus, we have identified a mechanism that underlies postsynaptic maturation, with important implications for neuromuscular function.

The development and maintenance of NMJs are regulated by both *trans*-synaptic and muscle intrinsic signaling mechanisms. Ephexin1 is expressed at both the presynaptic nerve terminus and the postsynaptic muscle membrane (Shamah et al., 2001). In this study, we provide evidence that the defects in postsynaptic maturation and neuromuscular transmission observed in *ephexin1*$^{-/-}$ mice are predominantly due to deficiency in muscle ephexin1-mediated signaling. First, the frequency of MEPPs in *ephexin1*$^{-/-}$ mice is similar to that of wild-type littermates, suggesting normal spontaneous neurotransmitter release in these mutant mice (data not shown). Second, despite the aberrant maturation of AChR clusters, gross morphological changes are not apparent at presynaptic terminals in *ephexin1*$^{-/-}$ mice during postnatal development or in the adult (Figures 2A and S3). Moreover, the transition from poly- to single-motor neuron innervation of the muscle fibers was not affected in *ephexin1*$^{-/-}$ mice, suggesting that synapse elimination occurs normally in the *ephexin1*$^{-/-}$ mice (Figures S3B and S3C) (Wyatt and Balice-Gordon, 2003). Importantly, the requirement of muscle ephexin1 is further demonstrated by the results of manipulating the expression of ephexin1 in muscle during early postnatal stages. In vivo knockdown of ephexin1 in wild-type mouse muscle inhibits the maturation of AChR clusters, whereas re-expression of ephexin1 in *ephexin1*$^{-/-}$ muscle restores the normal topological transformation of AChR clusters, allowing the formation of elaborately branched AChR clusters (Figures 4A–4D). We further showed that knockdown of ephexin1 in aneural myotubes perturbs the maturation of AChR clusters. Thus, our findings provide a mechanistic basis for the nerve-independent topological maturation of AChR clusters (Kummer et al., 2004). It is noteworthy that we have previously demonstrated an important role of ephexin1 in regulating dendritic spine retraction at CNS synapses (Fu et al., 2007). Our present study provides evidence that ephexin1 is also involved in the stabilization of neurotransmitter receptors at peripheral synapses. Notably, a recent study showed that ephexin1 at the presynaptic site of the *Drosophila* NMJ is involved in the homeostatic modulation of neurotransmitter release (Frank et al., 2009). Thus, it would be interesting to explore whether ephexin1 or its related members could exert similar functions at the presynaptic terminals of the mammalian NMJs.

Transformation of AChR clusters from a plaque-like shape to the elaborate arrays of branches requires selective stabilization of certain AChR regions and the disassembly of the others. This change in AChR patterning results in the concentration of AChR clusters juxtaposed to the motor nerve terminals, which ensures the efficacy of neurotransmission. AChR clusters are

tightly associated with the F-actin cytoskeleton, where actin polymerization is important for the formation and stabilization of NMJs (Dai et al., 2000; Hoch et al., 1994). As important regulators of actin cytoskeletal dynamics, Rho family GTPases control the formation of agrin-induced AChR clusters in myotubes in a precise and coordinated manner (Weston et al., 2000, 2003). However, the in vivo role of Rho GTPases in AChR stabilization during maturation of the NMJs is largely unknown. Our study reveals a critical involvement of an upstream regulator of Rho family GTPases at vertebrate NMJs, suggesting that the precise regulation of Rho GTPases is important for the maturation of NMJs.

Members of Rho family GTPases regulate various cellular functions through reorganization of the actin cytoskeleton. For example, Rac1 and Cdc42 activation leads to F-actin polymerization within the growth cones of neuronal cells, thus providing the protrusive activity for axonal growth. In contrast, activation of RhoA/ROCK depolymerizes F-actins locally in growth cones and generates contractile forces for growth cone collapse and axon retraction (Dickson, 2001; Gallo, 2006). Our findings showed that activation of RhoA downstream of ephexin1 leads to the destabilization of AChR clusters. ROCK activity is possibly involved in this process because inhibition of ROCK activity blocked ephrin-induced dispersal of AChR clusters (Figures S5A and S5B). However, inhibition of ROCK activity did not affect the basal AChR cluster number after agrin withdrawal, suggesting that there are possibly other downstream effectors of RhoA involved in ephexin1-dependent destabilization of AChR clusters. It has been reported that RhoA-dependent reorganization of actin cytoskeleton regulates endocytic pathways (Qualmann and Mellor, 2003), and the removal of AChR clusters from postsynaptic membrane is suggested to be regulated by the internalization of the receptors, which depends on actin polymerization (Bruneau and Akaaboune, 2006; Kumari et al., 2008; St John and Gordon, 2001). Indeed, we found that actin cytoskeletal rearrangements are involved in ephexin1-dependent shaping of AChR clusters, because the linkage of AChRs to the cytoskeleton was potentiated in ephexin1-knockdown myotubes (Figures 5C–5F). Hence, it is possible that ephexin1-dependent activation of RhoA reorganizes the local dynamics of the actin cytoskeleton and thus weakens the linkage between the receptors and F-actins and facilitates the disassembly of AChR clusters through internalization.

Because the enhancement of ephexin1 GEF activity toward RhoA is dependent on the phosphorylation of ephexin1 at Tyr[87], it is conceivable that regulation of ephexin1 at the NMJ requires upstream regulators. One likely candidate is EphA4. In addition to the localization of EphA4 and its ligands at the NMJ during early postnatal stages and its association with the actin-binding protein cortactin in muscle (Lai et al., 2001), EphA4 recruits and phosphorylates ephexin1 in a ligand-dependent manner (Fu et al., 2007; Sahin et al., 2005). Moreover, EphA4 interacts with ephexin1 upon activation and is required for ephrin-A1-induced AChR dispersal in cultured myotubes (Figures S5C–S5E). The morphology of NMJs in adult $EphA4^{-/-}$ mice, however, is indistinguishable from that of those in wild-type mice (Figure S5F), likely due to the ability of other Eph receptors to compensate for the loss of EphA4 function. In this context, it is noteworthy that EphA7 is developmentally regulated in skeletal muscle and is concentrated at the adult NMJ (Lai et al., 2001). Interestingly, ephexin1 activity is regulated by various signaling pathways upon Eph activation. Indeed, two protein kinases, SFKs and Cdk5, have been reported to phosphorylate ephexin1 and enhance its activity toward RhoA upon EphA4 activation (Fu and Ip, 2007; Fu et al., 2007; Sahin et al., 2005). In addition, these two kinases are able to exert their distinct functions in the stabilization of AChR clusters (Fu et al., 2005; Lin et al., 2005; Mohamed et al., 2001). Thus, further studies are required to resolve how these signaling proteins may function in concert to control the postsynaptic maturation of NMJs. Coordinated regulation of Rho GTPases by various Rho GTPase regulators has been reported in EphA4-dependent signaling (Cowan et al., 2005; Fu et al., 2007; Shi et al., 2007). It will be interesting to investigate if additional Rho GTPase regulators are involved in the postsynaptic maturation of NMJs. Together, our findings from $ephexin1^{-/-}$ mice and ephexin1-knockdown C2C12 myotubes have provided compelling evidence that ephexin1 is indispensable for precise neurotransmission at the NMJ through structural maturation of the postsynaptic apparatus.

EXPERIMENTAL PROCEDURES

Antibodies and Chemicals

Antibodies against α-tubulin and synaptophysin were purchased from Sigma; neurofilament antibody, from Chemicon; phosphotyrosine antibody (4G10), from Millipore; and RhoA antibody, from Santa Cruz. p-Eph and ephexin1 antibodies have been previously described (Fu et al., 2007). Antibody against AChRβ subunit (mAB 124) was a generous gift from Dr. J. Lindstrom (University of Pennsylvania Medical School, Philadelphia, PA). Alexa Fluor 555- and biotin-conjugated α-bungarotoxin (α-BTX) was purchased from Molecular Probes, and recombinant agrin was from R&D Systems.

Muscle Strength Measurement and Motor Behavioral Test

Adult $ephexin1^{-/-}$ mice and their wild-type littermates (Sahin et al., 2005) aged 2 to 4 months were subjected to the behavioral tests. Muscle fatigue resistance and motor coordination of the mice were measured using a rotating rod apparatus (Rota-Rod LE8200, Panlab). The test was performed by placing the mice on a motionless rod for 1 min. The rotating speed of the rod was then increased to 40 rpm in 5 min. The latency for the mice to fall off from the rod was recorded. The mice were subjected to the trials for 5 days, and three trials with intertrial intervals of 0.5 hr were given each day. Forelimb muscle strength was evaluated using an inverted screen test (Nishimune et al., 2008). Briefly, the mice were placed on a screen of wire mesh consisting of 1.5 mm-diameter wires, with their hindpaws wrapped in adhesive tapes. The screen was then elevated to 50 cm above the stage and inverted smoothly to let the mice hang by gripping the wire using their forepaws. The time over which the mice remained hanging on the screen was recorded.

Electrophysiology

Hemidiaphragms were dissected from adult wild-type and $ephexin1^{-/-}$ mice and placed in oxygenated NMJ solution (Fu et al., 2005). The resting membrane potential and spontaneous MEPPs were recorded by sharp microelectrodes via a microelectrode amplifier (Axoclamp 2B, Molecular Devices). At the end of the experiment, the presence of functional AChRs was tested by bath application of the agonist carbachol (50 μM). All experiments were performed at room temperature. Data were collected by the Digidata-pClamp package (Molecular Devices). Various parameters of the MEPPs including the amplitude and kinetics were analyzed by MiniAnalysis software (ver 5.1, Synaptosoft).

Immunohistochemical Analysis

Whole-mount staining of diaphragm, teased sternomastoid muscle, or tibialis anterior muscle was performed using synaptophysin/neurofilament (NF) antibodies and α-BTX as previously described (Froehner et al., 1990). Z-serial images of ∼10–20 layers (1 μm for each layer) were collected by confocal microscope (BX61, Olympus, Japan; 10X magnification for diaphragm; 63X for sternomastoid or tibialis anterior muscle) and presented as single-plane projections. All the quantification analysis was performed on en face images using Metamorph IMAGE ANALYSIS software (Universal Imaging). The degree of colocalization between nerve terminals and AChR clusters was measured. Briefly, regions of NMJs were selected and the background signals were subtracted. Colocalization of synaptophysin/NF (green) and AChR (red) was expressed as percentage of red pixels colocalizing with green pixels, or vice versa. The AChR area was measured as the area labeled with α-BTX (red), and the NMJ area refers to the total area that covers the entire AChR regions including the internal AChR-free space.

For in vivo transfection studies, 8 μg of GFP and 20 μg of ephexin1 cDNA construct or pSUPER ephexin1 (in 4 μl) were injected into tibialis anterior muscle of 1-week-old mice (Fu et al., 2001). AChR morphology was examined at P18.

Electron Microscopy

Transmission electron microscopy was performed as previously reported (Wang et al., 2007). Briefly, adult wild-type or *ephexin1*$^{-/-}$ mice was transcardially perfused with saline (0.9% NaCl) followed by 4% paraformaldehyde in PBS. Tibialis anterior muscles were dissected and teased into fibers with a diameter of ∼1 mm. These muscle fibers were then incubated in PBS containing α-BTX (1:500) for 20 min, and endplate-containing tissue blocks were dissected under fluorescence microscope and postfixed overnight at 4°C in 2% paraformaldehyde and 2% glutaraldehyde in PBS. Tissue blocks were then incubated in 2% osmium tetroxide for 2 hr, washed, and incubated with 2% uranylacetate for 2 hr. Tissue blocks were dehydrated, and then embedded in Spurr's resin (Electron Microscopy Sciences). Ultrathin sections (70 nm) were cut on an Ultratome (Leica, Reichert Ultracuts), and poststained with aqueous uranyl acetate/lead citrate. The observations were performed with a Hitachi H-7650 TEM operating at 80 kV. The pictures were taken with a Hitachi AMT XR-40 CCD camera.

Myotube Cultures, Transfection, and AChR Clustering

Mouse C2C12 myoblasts were cultured in DMEM supplemented with 20% FBS, and were differentiated into myotubes after the medium was switched to DMEM supplemented with 2% horse serum. C2C12 myotubes that were differentiated for 2 days were transfected with ephexin1 siRNA or its corresponding scramble siRNAs using Lipofectamine 2000 (Invitrogen). Knockdown of protein in muscle was found to last for at least 3 days. Similarly, differentiated C2C12 myotubes were transfected with mRNAs encoding for specific proteins using Lipofectamine 2000. The success of mRNA transfection was confirmed by the expression of GFP in C2C12 myotubes after transfection with GFP mRNA for ∼4 hr (with ∼90% efficiency).

Differentiated C2C12 myotubes were treated with agrin (10 ng/ml) for 16 hr to induce clustering of AChRs, which were then stained using α-BTX. For studies on the stability of preexisting AChR clusters, myotubes were first treated with agrin for 8 hr, and the AChRs were labeled with α-BTX. The myotubes were then washed twice with medium and maintained in agrin-free medium for another 12–14 hr. For clustering of ephrin-A1, ephrin-A1-Fc (R&D Systems) or Fc (Jackson Immunoresearch Labs) were preclustered with goat or mouse antibody to human Fc (Jackson Immunoresearch Labs) at a ratio of 1:5, and incubated at room temperature for 45 min before use. Myotubes were treated with ephrin-Fc or Fc at a concentration of 5 μg/ml.

For the quantification of AChR clusters, AChR clusters from ∼10 random fields per dish were imaged using fluorescence microscopy (n ≥ 3 dishes; 40X magnification; Leica, Germany). The number of AChR clusters was quantified using Metamorph IMAGE ANALYSIS software. Only AChR clusters with length ≥5 μm were counted.

To induce pretzel-like clusters, C2C12 myoblasts were cultured and differentiated on laminin-coated dishes as previously described (Kummer et al.,

2004). The morphology of AChR clusters was examined on myotubes that were differentiated for 3–6 days.

The AChR extractability assay and measurement of tyrosine-phosphorylated (pTyr) AChRβ were performed as described (Sadasivam et al., 2005). Briefly, the myotubes were extracted by a lysis buffer containing a final concentration of 0.05% Triton X-100. The lysate was then centrifuged, and the supernatants (0.05% fraction) were collected. The pellets were then re-extracted with a lysis buffer containing 1% Triton X-100. The supernatant (1% fraction) was then collected after centrifugation. The AChRs were precipitated from the lysate using biotin-conjugated α-BTX, followed by western blot analysis for AChRβ subunit. For the measurement of p-Tyr AChRβ, the myotubes were extracted by a lysis buffer containing 1% NP-40, precipitated using α-BTX, and subjected to western blot analysis for p-Tyr AChRβ (using 4G10 antibody).

RhoA Activation Assay

For details, see Supplemental Experimental Procedures.

SUPPLEMENTAL INFORMATION

Supplemental Information for this article includes five figures, one table, and Supplemental Experimental Procedures and can be found with this article online at doi:10.1016/j.neuron.2010.01.012.

REFERENCES

Adams, M.E., Kramarcy, N., Fukuda, T., Engel, A.G., Sealock, R., and Froehner, S.C. (2004). Structural abnormalities at neuromuscular synapses lacking multiple syntrophin isoforms. J. Neurosci. *24*, 10302–10309.

Balice-Gordon, R.J., and Lichtman, J.W. (1993). In vivo observations of pre- and postsynaptic changes during the transition from multiple to single innervation at developing neuromuscular junctions. J. Neurosci. *13*, 834–855.

Balice-Gordon, R.J., and Lichtman, J.W. (1994). Long-term synapse loss induced by focal blockade of postsynaptic receptors. Nature *372*, 519–524.

Borges, L.S., and Ferns, M. (2001). Agrin-induced phosphorylation of the acetylcholine receptor regulates cytoskeletal anchoring and clustering. J. Cell Biol. *153*, 1–12.

Bruneau, E.G., and Akaaboune, M. (2006). The dynamics of recycled acetylcholine receptors at the neuromuscular junction in vivo. Development *133*, 4485–4493.

Chevessier, F., Girard, E., Molgó, J., Bartling, S., Koenig, J., Hantaï, D., and Witzemann, V. (2008). A mouse model for congenital myasthenic syndrome due to MuSK mutations reveals defects in structure and function of neuromuscular junctions. Hum. Mol. Genet. *17*, 3577–3595.

Cowan, C.W., Shao, Y.R., Sahin, M., Shamah, S.M., Lin, M.Z., Greer, P.L., Gao, S., Griffith, E.C., Brugge, J.S., and Greenberg, M.E. (2005). Vav family GEFs link activated Ephs to endocytosis and axon guidance. Neuron *46*, 205–217.

Dai, Z., Luo, X., Xie, H., and Peng, H.B. (2000). The actin-driven movement and formation of acetylcholine receptor clusters. J. Cell Biol. *150*, 1321–1334.

Dickson, B.J. (2001). Rho GTPases in growth cone guidance. Curr. Opin. Neurobiol. *11*, 103–110.

Frank, C.A., Pielage, J., and Davis, G.W. (2009). A presynaptic homeostatic signaling system composed of the Eph receptor, ephexin, Cdc42, and CaV2.1 calcium channels. Neuron *61*, 556–569.

Froehner, S.C., Luetje, C.W., Scotland, P.B., and Patrick, J. (1990). The post-synaptic 43K protein clusters muscle nicotinic acetylcholine receptors in Xenopus oocytes. Neuron *5*, 403–410.

Fu, A.K., and Ip, N.Y. (2007). Cyclin-dependent kinase 5 links extracellular cues to actin cytoskeleton during dendritic spine development. Cell Adh. Migr. *1*, 110–112.

Fu, A.K., Fu, W.Y., Cheung, J., Tsim, K.W., Ip, F.C., Wang, J.H., and Ip, N.Y. (2001). Cdk5 is involved in neuregulin-induced AChR expression at the neuromuscular junction. Nat. Neurosci. *4*, 374–381.

Fu, A.K., Ip, F.C., Fu, W.Y., Cheung, J., Wang, J.H., Yung, W.H., and Ip, N.Y. (2005). Aberrant motor axon projection, acetylcholine receptor clustering, and neurotransmission in cyclin-dependent kinase 5 null mice. Proc. Natl. Acad. Sci. USA *102*, 15224–15229.

Fu, W.Y., Chen, Y., Sahin, M., Zhao, X.S., Shi, L., Bikoff, J.B., Lai, K.O., Yung, W.H., Fu, A.K., Greenberg, M.E., and Ip, N.Y. (2007). Cdk5 regulates EphA4-mediated dendritic spine retraction through an ephexin1-dependent mechanism. Nat. Neurosci. *10*, 67–76.

Gallo, G. (2006). RhoA-kinase coordinates F-actin organization and myosin II activity during semaphorin-3A-induced axon retraction. J. Cell Sci. *119*, 3413–3423.

Grady, R.M., Zhou, H., Cunningham, J.M., Henry, M.D., Campbell, K.P., and Sanes, J.R. (2000). Maturation and maintenance of the neuromuscular synapse: genetic evidence for roles of the dystrophin—glycoprotein complex. Neuron *25*, 279–293.

Hoch, W., Campanelli, J.T., and Scheller, R.H. (1994). Agrin-induced clustering of acetylcholine receptors: a cytoskeletal link. J. Cell Biol. *126*, 1–4.

Kong, L., Wang, X., Choe, D.W., Polley, M., Burnett, B.G., Bosch-Marcé, M., Griffin, J.W., Rich, M.M., and Sumner, C.J. (2009). Impaired synaptic vesicle release and immaturity of neuromuscular junctions in spinal muscular atrophy mice. J. Neurosci. *29*, 842–851.

Kumari, S., Borroni, V., Chaudhry, A., Chanda, B., Massol, R., Mayor, S., and Barrantes, F.J. (2008). Nicotinic acetylcholine receptor is internalized via a Rac-dependent, dynamin-independent endocytic pathway. J. Cell Biol. *181*, 1179–1193.

Kummer, T.T., Misgeld, T., Lichtman, J.W., and Sanes, J.R. (2004). Nerve-independent formation of a topologically complex postsynaptic apparatus. J. Cell Biol. *164*, 1077–1087.

Lai, K.O., Ip, F.C., Cheung, J., Fu, A.K., and Ip, N.Y. (2001). Expression of Eph receptors in skeletal muscle and their localization at the neuromuscular junction. Mol. Cell. Neurosci. *17*, 1034–1047.

Lai, K.O., Chen, Y., Po, H.M., Lok, K.C., Gong, K., and Ip, N.Y. (2004). Identification of the Jak/Stat proteins as novel downstream targets of EphA4 signaling in muscle: implications in the regulation of acetylcholinesterase expression. J. Biol. Chem. *279*, 13383–13392.

Lanuza, M.A., Garcia, N., Santafé, M., González, C.M., Alonso, I., Nelson, P.G., and Tomàs, J. (2002). Pre- and postsynaptic maturation of the neuromuscular junction during neonatal synapse elimination depends on protein kinase C. J. Neurosci. Res. *67*, 607–617.

Lee, C.W., Han, J., Bamburg, J.R., Han, L., Lynn, R., and Zheng, J.Q. (2009). Regulation of acetylcholine receptor clustering by ADF/cofilin-directed vesicular trafficking. Nat. Neurosci. *12*, 848–856.

Lin, W., Dominguez, B., Yang, J., Aryal, P., Brandon, E.P., Gage, F.H., and Lee, K.F. (2005). Neurotransmitter acetylcholine negatively regulates neuromuscular synapse formation by a Cdk5-dependent mechanism. Neuron *46*, 569–579.

Linnoila, J., Wang, Y., Yao, Y., and Wang, Z.Z. (2008). A mammalian homolog of Drosophila tumorous imaginal discs, Tid1, mediates agrin signaling at the neuromuscular junction. Neuron *60*, 625–641.

Luo, Z.G., Wang, Q., Zhou, J.Z., Wang, J., Luo, Z., Liu, M., He, X., Wynshaw-Boris, A., Xiong, W.C., Lu, B., and Mei, L. (2002). Regulation of AChR clustering by Dishevelled interacting with MuSK and PAK1. Neuron *35*, 489–505.

Luo, Z.G., Je, H.S., Wang, Q., Yang, F., Dobbins, G.C., Yang, Z.H., Xiong, W.C., Lu, B., and Mei, L. (2003). Implication of geranylgeranyltransferase I in synapse formation. Neuron *40*, 703–717.

Luo, S., Zhang, B., Dong, X.P., Tao, Y., Ting, A., Zhou, Z., Meixiong, J., Luo, J., Chiu, F.C., Xiong, W.C., and Mei, L. (2008). HSP90 beta regulates rapsyn turnover and subsequent AChR cluster formation and maintenance. Neuron *60*, 97–110.

Marques, M.J., Conchello, J.-A., and Lichtman, J.W. (2000). From plaque to pretzel: fold formation and acetylcholine receptor loss at the developing neuromuscular junction. J. Neurosci. *20*, 3663–3675.

Mitsui, T., Kawajiri, M., Kunishige, M., Endo, T., Akaike, M., Aki, K., and Matsumoto, T. (2000). Functional association between nicotinic acetylcholine receptor and sarcomeric proteins via actin and desmin filaments. J. Cell. Biochem. *77*, 584–595.

Mohamed, A.S., Rivas-Plata, K.A., Kraas, J.R., Saleh, S.M., and Swope, S.L. (2001). Src-class kinases act within the agrin/MuSK pathway to regulate acetylcholine receptor phosphorylation, cytoskeletal anchoring, and clustering. J. Neurosci. *21*, 3806–3818.

Moransard, M., Borges, L.S., Willmann, R., Marangi, P.A., Brenner, H.R., Ferns, M.J., and Fuhrer, C. (2003). Agrin regulates rapsyn interaction with surface acetylcholine receptors, and this underlies cytoskeletal anchoring and clustering. J. Biol. Chem. *278*, 7350–7359.

Nishimune, H., Valdez, G., Jarad, G., Moulson, C.L., Müller, U., Miner, J.H., and Sanes, J.R. (2008). Laminins promote postsynaptic maturation by an autocrine mechanism at the neuromuscular junction. J. Cell Biol. *182*, 1201–1215.

Qualmann, B., and Mellor, H. (2003). Regulation of endocytic traffic by Rho GTPases. Biochem. J. *371*, 233–241.

Sadasivam, G., Willmann, R., Lin, S., Erb-Vögtli, S., Kong, X.C., Rüegg, M.A., and Fuhrer, C. (2005). Src-family kinases stabilize the neuromuscular synapse in vivo via protein interactions, phosphorylation, and cytoskeletal linkage of acetylcholine receptors. J. Neurosci. *25*, 10479–10493.

Sahin, M., Greer, P.L., Lin, M.Z., Poucher, H., Eberhart, J., Schmidt, S., Wright, T.M., Shamah, S.M., O'connell, S., Cowan, C.W., et al. (2005). Eph-dependent tyrosine phosphorylation of ephexin1 modulates growth cone collapse. Neuron *46*, 191–204.

Sanes, J.R., and Lichtman, J.W. (2001). Induction, assembly, maturation and maintenance of a postsynaptic apparatus. Nat. Rev. Neurosci. *2*, 791–805.

Selcen, D., Milone, M., Shen, X.M., Harper, C.M., Stans, A.A., Wieben, E.D., and Engel, A.G. (2008). Dok-7 myasthenia: phenotypic and molecular genetic studies in 16 patients. Ann. Neurol. *64*, 71–87.

Shamah, S.M., Lin, M.Z., Goldberg, J.L., Estrach, S., Sahin, M., Hu, L., Bazalakova, M., Neve, R.L., Corfas, G., Debant, A., and Greenberg, M.E. (2001). EphA receptors regulate growth cone dynamics through the novel guanine nucleotide exchange factor ephexin. Cell *105*, 233–244.

Shi, L., Fu, W.Y., Hung, K.W., Porchetta, C., Hall, C., Fu, A.K., and Ip, N.Y. (2007). Alpha2-chimaerin interacts with EphA4 and regulates EphA4-dependent growth cone collapse. Proc. Natl. Acad. Sci. USA *104*, 16347–16352.

Slater, C.R. (1982). Postnatal maturation of nerve-muscle junctions in hindlimb muscles of the mouse. Dev. Biol. *94*, 11–22.

Slater, C.R. (2008). Structural factors influencing the efficacy of neuromuscular transmission. Ann. N Y Acad. Sci. *1132*, 1–12.

Slater, C.R., Fawcett, P.R., Walls, T.J., Lyons, P.R., Bailey, S.J., Beeson, D., Young, C., and Gardner-Medwin, D. (2006). Pre- and post-synaptic

abnormalities associated with impaired neuromuscular transmission in a group of patients with 'limb-girdle myasthenia'. Brain *129*, 2061–2076.

St John, P.A., and Gordon, H. (2001). Agonists cause endocytosis of nicotinic acetylcholine receptors on cultured myotubes. J. Neurobiol. *49*, 212–223.

Wang, J., Li, Y., Lo, S.W., Hillmer, S., Sun, S.S., Robinson, D.G., and Jiang, L. (2007). Protein mobilization in germinating mung bean seeds involves vacuolar sorting receptors and multivesicular bodies. Plant Physiol. *143*, 1628–1639.

Weston, C., Yee, B., Hod, E., and Prives, J. (2000). Agrin-induced acetylcholine receptor clustering is mediated by the small guanosine triphosphatases Rac and Cdc42. J. Cell Biol. *150*, 205–212.

Weston, C., Gordon, C., Teressa, G., Hod, E., Ren, X.D., and Prives, J. (2003). Cooperative regulation by Rac and Rho of agrin-induced acetylcholine receptor clustering in muscle cells. J. Biol. Chem. *278*, 6450–6455.

Wyatt, R.M., and Balice-Gordon, R.J. (2003). Activity-dependent elimination of neuromuscular synapses. J. Neurocytol. *32*, 777–794.